American Journal of Mechanical and Industrial Engineering
2023; 8(1): 7-17
http://www.sciencepublishinggroup.com/j/ajmie
doi: 10.11648/j.ajmie.20230801.12
ISSN: 2575-6079 (Print); ISSN: 2575-6060 (Online)

Finite Element Simulation to Optimize the Mechanical Properties and Deformation of the Bevel Joint of 9.25 mm Thick Aluminum 6061-T6 with only One Pass

Milad Bahrami, Michel Guillot

PI2/REGAL Research Team, Department of Mechanical Engineering, Laval University, Quebec, Canada

Email address:
milad.bahrami.1@ulaval.ca (Milad Bahrami)

To cite this article:
Milad Bahrami, Michel Guillot. Finite Element Simulation to Optimize the Mechanical Properties and Deformation of the Bevel Joint of 9.25 mm Thick Aluminum 6061-t6 with only One Pass. *American Journal of Mechanical and Industrial Engineering.* Vol. 8, No. 1, 2023, pp. 7-17. doi: 10.11648/j.ajmie.20230801.12

Received: July 25, 2022; **Accepted**: May 18, 2023; **Published**: May 29, 2023

Abstract: In industrial settings, it is customary to employ at least a three-passes welding for 9.525 mm-thick welded samples, which results in increased angular distortion and longitudinal/transversal deformation. This study outlines the optimized welding parameters for a butt-welded joint V groove with a 60-degree bevel angle and a 2.5 mm root face, utilizing a single pass, on a 9.525 mm thick sample. The present investigation involved the development of a 3D computational model to examine the thermal characteristics and distortion distribution during the process of gas metal arc welding of the aluminium alloy 6061-T6. The present paper employed the Taguchi methodology to compute the thermal behaviour technique using orthogonal arrays, a well-established Design of Experiments (DOE) approach for finite element analysis (FEA). Additionally, an artificial neural network (ANN) model was employed to forecast distortion and stress. The study produced 3D surface graphs and contour plots to clarify the correlation between welding parameters, stress, and distortion. Following the determination of optimized parameters through finite element analysis (FEA), experimental tests were conducted to compare and validate the FEA outcomes. The present investigation has employed welding parameters, namely arc voltage (v), arc travel speed (mm/s), current (A), gun angle (degree), distance between the nozzle and weld (mm), and root gap (mm).

Keywords: Welding Parameters, Aluminum Alloy, Mechanical Properties, Distortion, Neural Modeling, Taguchi Method, Finite Element Analysis

1. Introduction

6061-T6 is a commonly used aluminium alloy worldwide. The material exhibits a favourable ratio of strength to weight and is amenable to thermal treatment. Irrespective of the form in which it is used, such as sheet, plate, bar, or angle, 6061 is the preferred material for a diverse array of applications. The aforementioned categories encompass various modes of transportation, such as boats and ships, as well as aircraft, in addition to structures such as bridges. These fields pertain to the domain of engineering and are utilised for their structural properties. This particular aluminium variant is classified as an alloy due to the presence of magnesium (1%) and silicon (0.6%) as its primary constituents. Because of this, it is very resistant to corrosion, stress, and breaking. This also means that the grade is easy to shape and easy to weld. Aluminum has a high thermal conductivity, which can cause it to distort and can have a big effect on how well it is welded. Aluminum is about five times better at moving heat than low-carbon steel. Gas metal arc welding is the type of welding used in this study (GMAW). Since it became commercially available, this process has become very important in the welding industry. During GMAW, a shielding gas keeps the arc welding from being affected by things in the air, and an electric arc provides the heat. [1, 2] There are many factors that affect the welding process and the results, such as arc voltage, current, arc travel speed, arc length, degree of gun angle, preheat temperature, wire feed speed, etc [3-5]. Figure 1 shows some of the most important parameters for welding.

In fact, control of these variables contributes to welding defects like deformations in the microstructure, the formation

of residual stresses in welded joints, and flaws on the surface, as well as a decrease in the welding process's productivity [6-10]. There are two ways to find out about welding residual stress and deformation: by doing an experiment or running a computer simulation [11-15]. There are several benefits to using FEA to simulate the welding process and validate it with experimental observations, such as the ability to predict thermal residual stress and temperature distribution in welding structures [15-17], and the possibility of including non-linear temperature-dependent aspects when modeling the highly complex multi-physics problems that are part of welding procedures [18-20]. At the design stage, less distortion can be achieved by reducing the size of the weld, optimizing the welding parameters, and changing the geometry of the weld joint. [21, 22] Several studies have been done to simulate welding residual stress and distortion distribution with a focus on the characteristics on top of residual stress distribution within a weldment's steady region and the distribution of welding residual stress [23-25]. Artificial neural network (ANN) models may remarkably build a mapping relationship between welding parameters and the resulting variables. This is made possible by the high self-learning and self-adaptation capabilities that these models possess. It was suggested that an ANN be used in order to determine a connection between the output outcomes and the welding parameters.

The goal of this work was to figure out how to use welding parameters to get the best mechanical properties and the least amount of distortion. In this search, Metal Inert Gas (MIG) welding is a flexible gas metal arc welding (GMAW) method for 9.525 mm thick plate. This study is mainly about how to find the best parameters for MIG welding. Aluminum 6061-T6 samples will be used for both FEA and experiments. The samples will have a V-groove butt joint configuration with a 60-degree bevel angle, a 2.5-mm root face, and a thickness of 9.525 mm. The Design of Experiments (DOE) for Finite Element Analysis (FEA) uses an Orthogonal Array (L8) based on the Taguchi method to find the best parameters. Then, a model called an artificial neural network (ANN) is used to predict the deformation and yield stress. For the results, 3D surface graphs and contour plots will be made to show how welding parameters, distortion, and yield stress are related to each other. Then, based on the results of the ANN model and FEA, experimental samples were welded, and the FEA and experimental results were compared. The ideal range of process parameters like voltage, wire feed speed, gun angle, distance between nozzle and weld, travel speed, root gap, and root face will be found. (Figure 1)

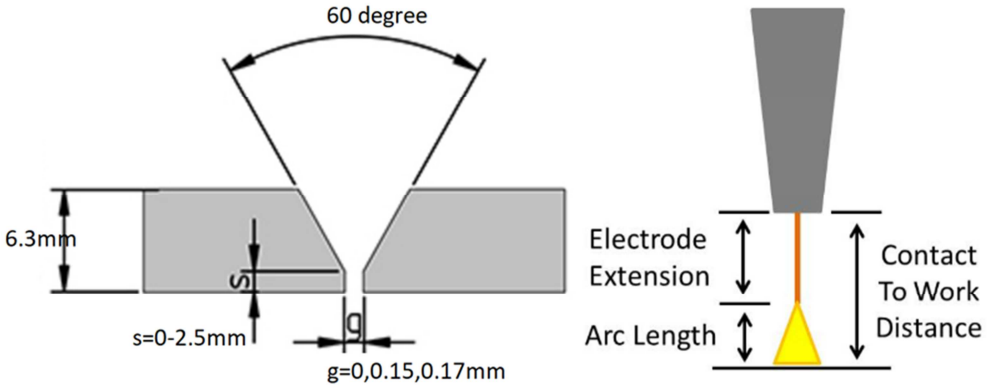

(a) (b)

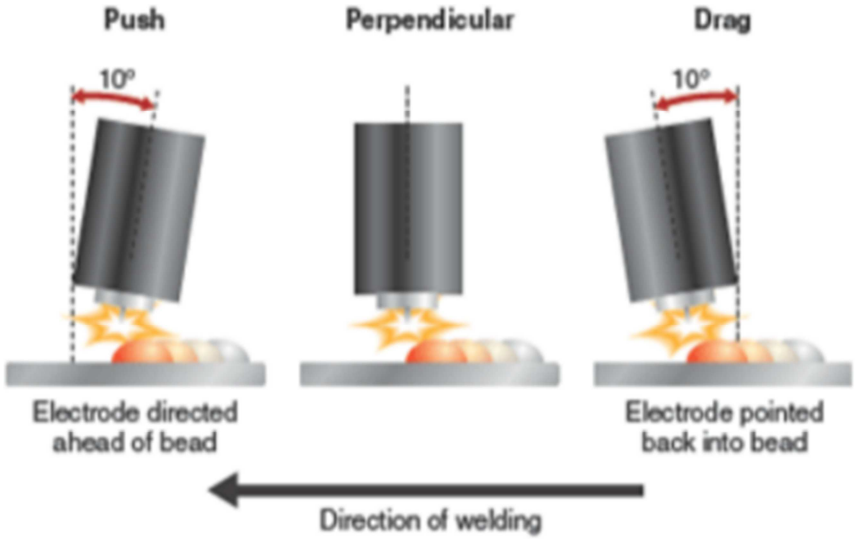

(c)

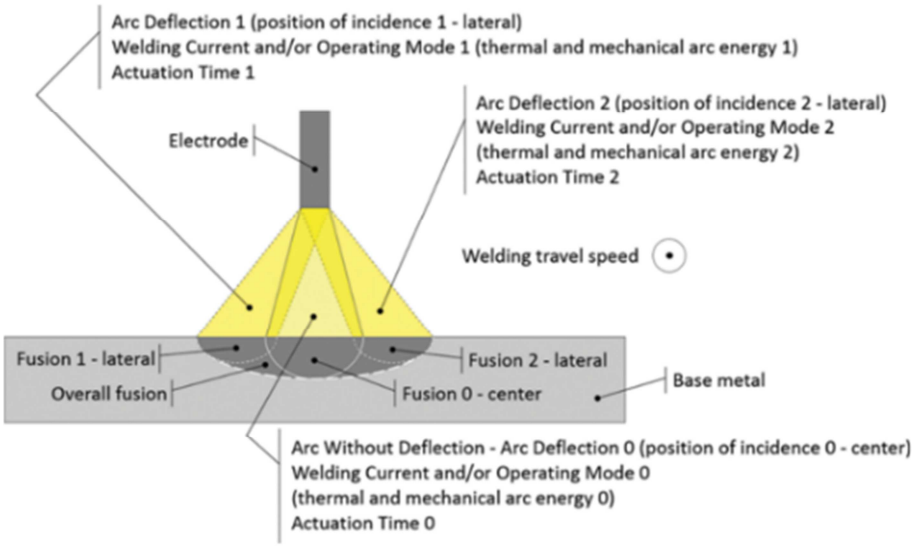

(d)

Figure 1. *(a) Geomwtry of joint (b) Distance between Nozzle to Weld (c) Gun Angle (d) Welding Process.*

2. Material and Method

2.1. Method

Test specimens measuring 9.525x76x254 mm with a bevel angle of 60 degrees have been fabricated and modelled. According to finite element analysis, the best welding parameters have the largest ultimate tensile stress and the least amount of deformation. To predict deformation and stresses, design of experiments (DOE) based on the Taguchi method, orthogonal array (L8), and artificial neural network (ANN) modelling are utilised. The ideal welding parameters of the ANN model have been simulated once more, and the output results have been determined. The best, optimal, average, and worst welding parameters were shown. The samples were then welded, and the results were compared with FEA. In the end, it was found that a 9.25-mm butt-welded sample had the least amount of distortion and the highest UTS with a single pass in the optimal range of welding parameters.

2.2. Experimental Procedure

Welding is one of the most important and widely used ways to put things together in the business world. To improve quality, it is important to know as much as possible about the shape, size, and residual stress of a welded piece. In this search study, four samples have been welded by the Fanuc R2000 robot (Figure 2a) and Miller Auto-Axcess 450 (Figure 2c) as a welding machines with pulsed arc welding technology. For experiment tests, distortion has been measured using a coordinate measuring machine (CMM). On the top surface of all the samples, 40 points were measured (X-Y-Z). Using the data, the best-fit plane was found, which is used as a guide for the rest of the data. (Figure 3a). In addition to investigating the mechanical properties, a tensile test of the weld joint was performed in accordance with the American Society for Testing and Materials (ASTM) B8M-04 standard. A hydraulic testing machine with a load cell that can measure up to 44.5 KN and is calibrated to 0.08 KN and a crosshead speed of 1 mm/min is utilized for the tensile test. (Figure 3b) All experiment samples have been evaluated by non-destructive tests (ultrasonic tests) and no surface or internal defect has been found.

2.3. Welding Material

The base metal is 6061-T6 aluminum, table 1a shows the material properties of the aluminum 6061-T6.

The material properties of this wire (5356, 1.2 mm) are shown in Table 1b, and 100% Argon is used for gas protection at a flow rate of 0.71 cubic meters per hour (m3/hr) (25 cfh).

Table 1. *Mechanical Properties and Chemical Composition Material properties of (a) aluminum 6061-T6 (b) wire 5356.*

(a)

	Chemical Composition (wt%)						
Material	Al	Mg	Mn	Cu	Fe	Si	UTS (MPa)
AA-6061-T6	Bal.	0.83	0.07	0.19	0.19	0.55	285

(b)

	Chemical Composition (wt%)							
Material	Al	Mg	Zn	Cu	Fe	Si	Other total	Shear moduls (GPa)
Wire 5356	92.9-95.3	4.5-5.5	0.1	0.10	0.4	0.25	0.15	26

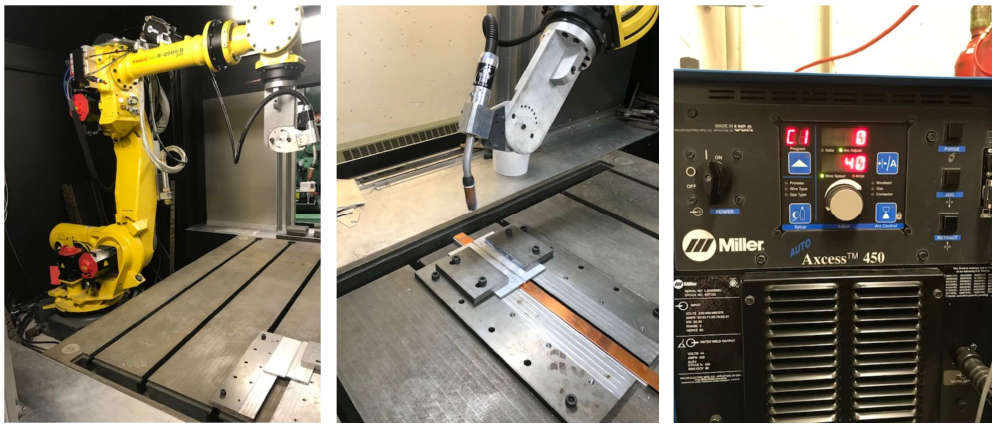

(a) (b) (c)

Figure 2. *(a) Fanuc R2000 robot (b) Schematic of the welding process (c) Miller Auto-Axcess 450.*

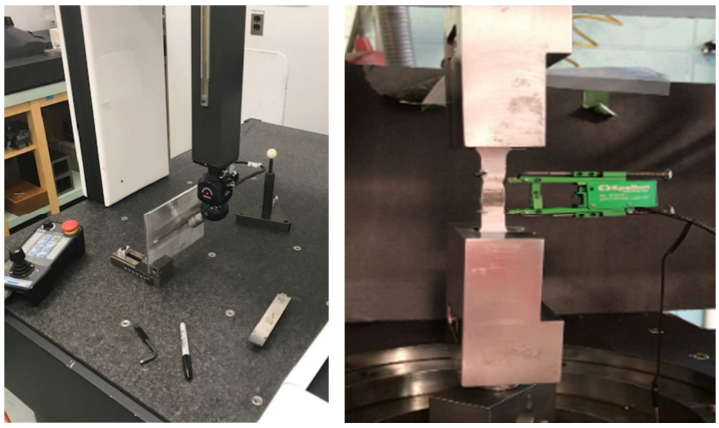

(a) (b)

Figure 3. *(a) CMM machine for distortion mesaurment (b) Schematic of the UTS mesaurment machine.*

3. Numerical Model and Finite Element Analysis

3.1. Geometry Modelling

The test specimens of 9.525x76x254 mm with a 60-degree bevel angle, different root gaps, and a root face of 2.5 mm in the weld zone are modelled, and a mesh is also created in NX software. The FEA model for the sample contains a total of 16472 hexahedral elements with 22084 associated nodes. The mesh grid is fine and uniform in the nearest regions of the weld seam where there are high temperatures and significant stress gradients, and it is coarse in the farthest regions. The maximum aspect ratio for mesh is 2.54 mm, and the percentage of elements with an aspect ratio of less than 2.5mm is almost 99.9%. Figure 4 shows the mesh for the test sample that has been created in NX software.

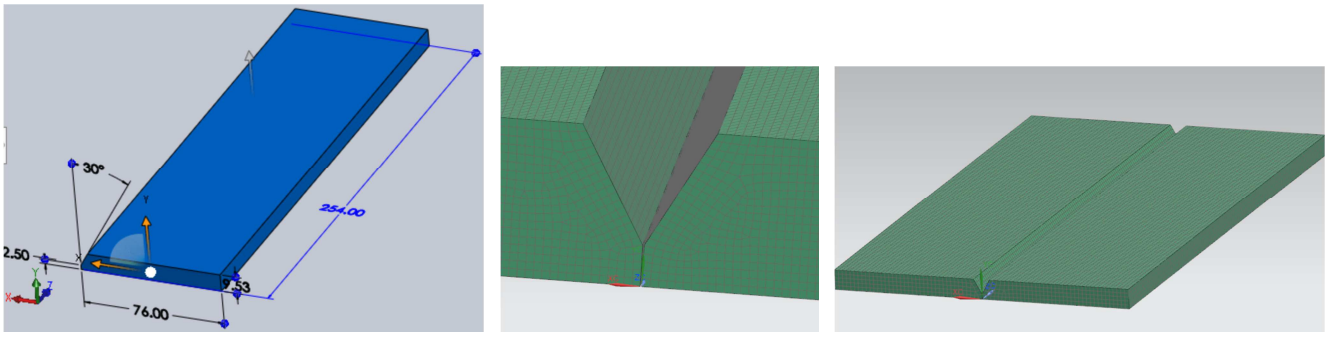

(a) (b) (c)

Figure 4. *Geometry of sample from NX for (a) Joint preparation (b) Meshed around weld zone (c) Meshed for completed sample.*

3.2. Simulation

A 3D mesh that was created in NX was transferred to Simufact welding simulation software to simulate the welding process and produce three configurations of butt weld joint samples. Simufact welding simulation software is used to simulate the welding and analyze the distortion and deformation. This finite element software is used for the simulation analysis of the weldment and it is necessary to define the solver, boundary conditions, heat resources, including welding parameters such as voltage, current, and travel speed, as well as gun angle, the distance of the nozzle to the weld, heat transfer coefficient parameters, and finally tracking of the welds. The solver is used with iterative sparse solver setting parameters including total simulation time, the respective flow time, time step, mesh refinement level, and the friction coefficient of the tracking point. From the Simufact software, the simulation was done with AL6061-T6, which has the same chemical composition as the Al6061 T6 in the experiment model. The process type is arc welding, the ambient temperature is 20°C, the components are 2 meshed samples converted from NX to Simufact, the fixing parts are exactly the same geometry as the experiments with the same dimension, and the acceleration due to gravity is 9.81 m/s2. Figure 5 shows samples with boundary conditions before starting solving and welding. Table 2 has been used for the first L8 DOE for FEA. In this table, the input welding parameters are arc voltage (V), travel speed (TS), wire feed speed (WFS), gun angle (GA), root gap (RG), and distance between nozzle and weld (DISW). The efficiency is 0.9 for arc welding [28]. The welding machine has been used to measure how well it uses heat input, which is also known as current (I).

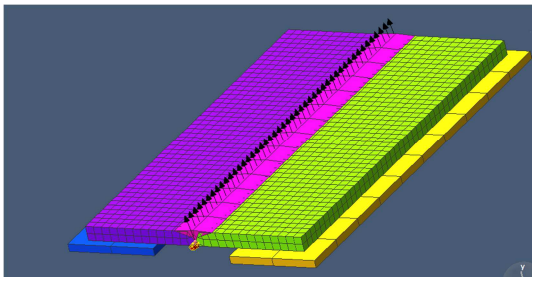

Figure 5. *Meshed sample with boundary condition.*

Table 2. *Comparison of actual weld and simulated weld.*

Test nu.	V	WFS	TS	GA	RG	DISW	Current	Energy per length
Unit	v	mm/s	mm/s	degree	mm	mm	A	J/cm
1	25	190	8	10	0	11	245	7656
2	25	190	8	11	0.127	13	250	7812
3	25	210	9	10	0	13	260	7222
4	25	210	9	11	0.127	11	265	7361
5	27	190	9	10	0.127	11	250	7500
6	27	190	9	11	0	11	245	7350
7	27	210	8	10	0.127	13	265	8943
8	27	210	8	11	0	11	260	8775
		L8 DOE						

4. Simulation Results

4.1. Thermal Simulation Results

In Simufact software [26], thermal results can be analyzed separately. Figure 6 shows the temperature field distribution of the weld pool during the numerical simulation of the arc welding. As seen in this figure, the temperature gradient of the weld zone is relatively high and the maximum temperature is 653°C. By measuring the end weld point of the simulated weld and the actual weld, the results are shown in Table 3. The error between simulation and actual welding is about 5%. So, there is a good match between the results of the calculated weld simulation and the results of the experiments. (Infrared radiation has been used for experimental temporal measurements.)

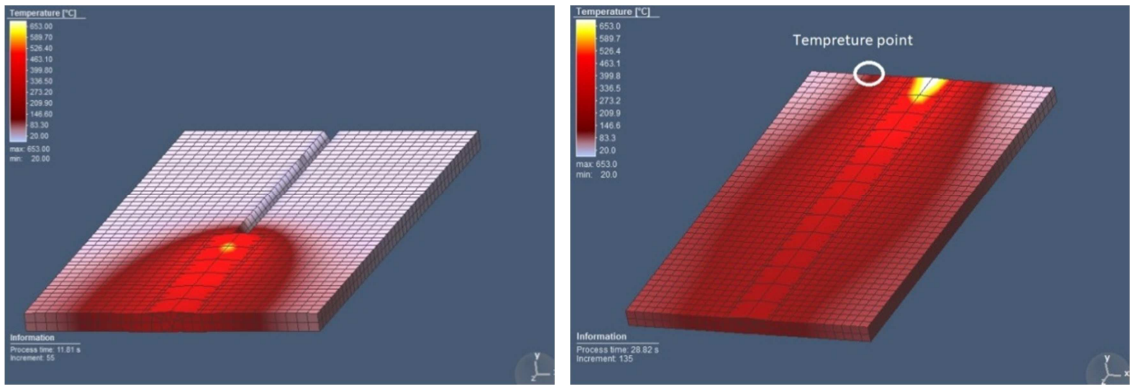

(a) (b)

(c) (d)

Figure 6. *Temperature distribution (a) midle of the weld (b) Temperature point after finish welding (140°C) (c) Sample before start weld (d) Temperature point from experiment after welding.*

Table 3. *Comparison of actual weld and simulated weld.*

Temperature for end point from experiment	Temperature for end point from FEA	Error
°C	°C	%
131.2	140	5

4.2. Distortion and Stresses Results

Table 4 shows the results from Simufact software for displacement, distortion, and stresses. Simufact figures out welding residual stresses using a model of an elastic-plastic material that changes with temperature and hardens. Most of the time, people don't think about how the properties of a material change at temperatures above its melting point. By defining the coefficient of thermal expansion correctly, the thermal expansion of the liquid phase can be stopped. At the same time, the effective plastic strains that describe the progression of hardening are set to zero until the temperature drops below the melting point of the material. This method is enough to figure out the distortions caused by welding for a wide range of metals. Residual stresses and tensile strength, on the other hand, are usually affected by more complicated laws of materials. Work hardening, softening due to grain coarsening in the melt pool, phase transformations (including hardening due to the formation of bainite and martensite, as well as transformation strains and transformation induced plasticity), dilution, and precipitation processes are all things that could change how a material behaves [27]. Figure 7 demonstrates how distortion affected the best and worst samples of the first DOE, and Figure 8 demonstrates how stress affected the best and worst samples of the second DOE.

Table 4. *Distortions and Stresses results from FEA.*

Test nu	Y Distortion	Yield stress	Effective stress	Normal Stress
Unit	mm	Mpa	Mpa	Mpa
1	0.37	162	160	206
2	0.52	159	160	202
3	0.4	162	163	209
4	0.38	162	158	188
5	0.37	159	158	197
6	0.64	160	160	201
7	0.43	160	160	203
8	0.39	159	159	207

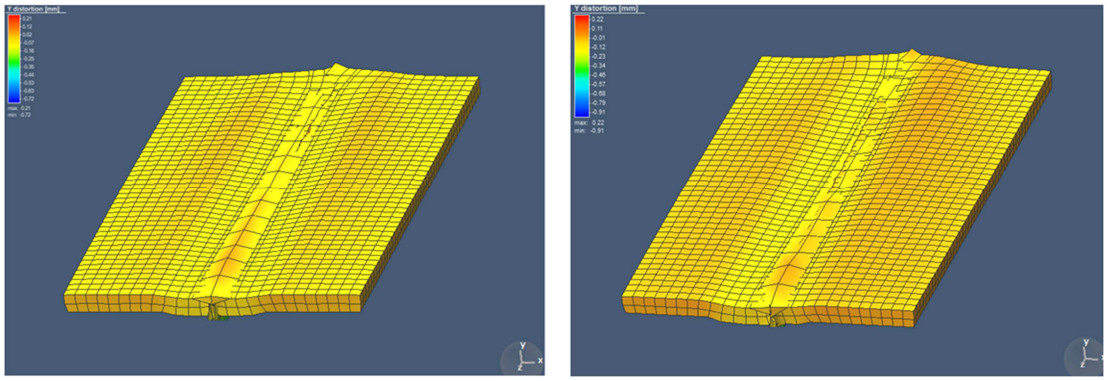

Y deformation: (-0.16 to +0.21) = 0.37 (a)

Y deformation: (-0.42 to +0.22) = 0.64 (b)

Figure 7. *Deformation distribution on Y axes from FEA (a) Best sample number 5 (b) Worst sample number 6.*

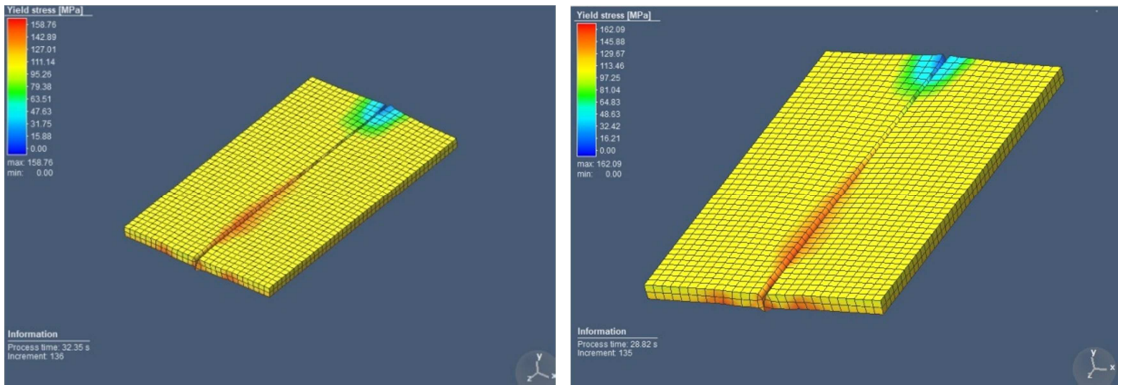

(a) (b)

Figure 8. *Yield stress distribution from FEA (a) Worst sample number 1 (b) Best sample number 3.*

5. Artificial Neural Network Modeling

The ANN model has been trained with the help of the results from the DOE. Welding parameters include voltage, wire feed speed, root gap, and the distance between the nozzle and the weld in the ANN model. Table 4 shows the learned data that will be used in the ANN model. Table 5 shows the RMSE and the maximum error for both the training data and the learned data.

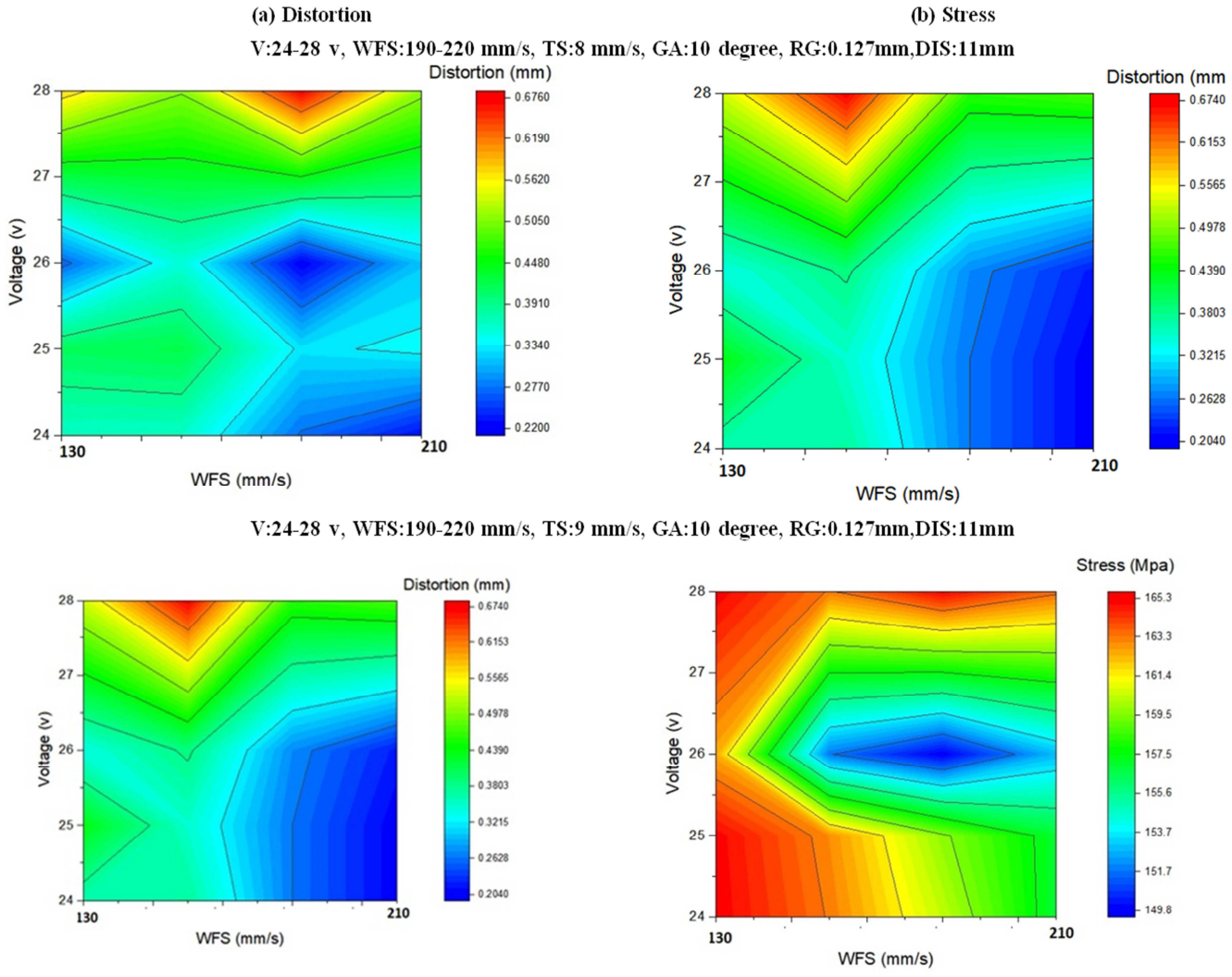

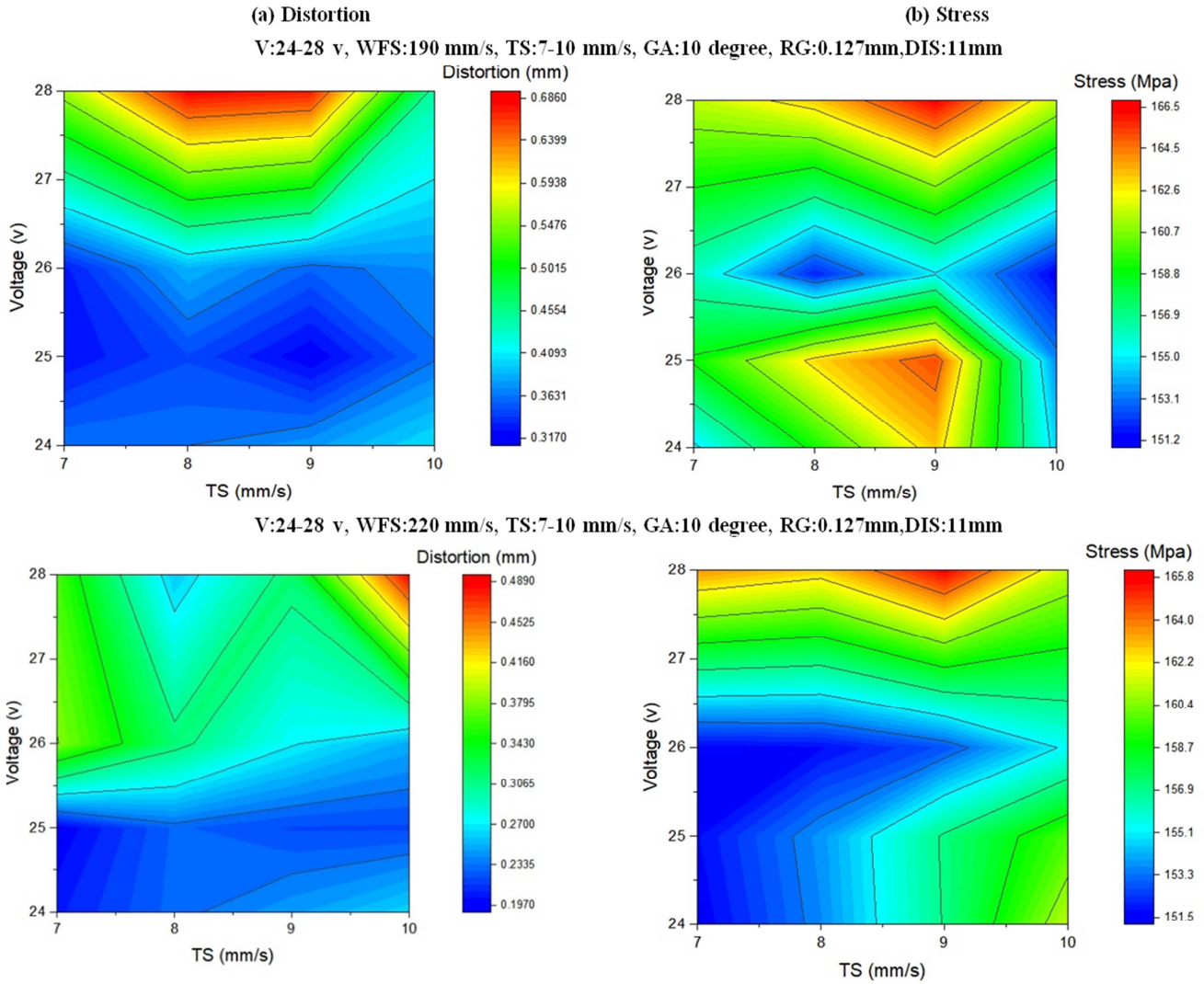

Figure 9. *Deformation distribution on Y axes from FEA (a) best sample number 5 (b) worst sample number 6.*

Table 5*. Trained data for ANN model.*

Test nu.	V	WFS	TS	GA	RG	DISW	Y Distortion	Yield stress
Unit	v	mm/s	mm/s	degree	mm	mm	mm	Mpa
1	25	190	8	10	0	11	0.40	162
2	25	190	8	11	0.127	13	0.52	159
3	25	210	9	10	0	13	0.43	162
4	25	210	9	11	0.127	11	0.38	162
5	27	190	9	10	0.127	13	0.37	159
6	27	190	9	11	0	11	0.64	160
7	27	210	8	10	0.127	13	0.43	160
8	27	210	8	11	0	11	0.39	159

The results of analyzing the data from ANN have been evaluated, and results for distortion (minimum) and stress (maximum) have been investigated, with 3D contour plots shown in Figure 9. In this figure, the comparison results of distortion and stress with a variation of voltage, WFS, and travel speed have been shown around optimized parameters. In Table 5, you can see the optimized parameters from the ANN model and the results from FEA for distortion and stress.

Table 6. *Optimized welding parameters and FEA results.*

V	WFS	TS	GA	RG	DISW	Distortion	Stress
v	mm/s	mm/s	degree	mm	mm	mm	Mpa
27	190-210	8-9	10	0.127	11	0.25	165

6. Experimental Results

The best and worst sample distortions from simulation (tests 5 and 6), one test from the average parameters of the simulation (test 7) and finally one test from optimizing parameters have been welded. Table 7 displays the experiment results for distortion and UTS measured by CMM machine and hydraulic machine for all four samples, as well as comparison experiment results with FEA results and error calculation. Figure 11 shows the three model of the distortion, of the best and worst samples.

(a) (b)

Figure 10. *Sample for the UTS measurement (a) Weld surface (b) Root weld (penetration).*

Table 7. *Comparison of the Experiments and FEA results.*

Test nu.	V	WFS	TS	GA	RG	DISW	FEA stress	Experiments stress	Error	FEA Distortion	Experiments Distortion	Error
Unit	v	mm/s	mm/s	degree	mm	mm	Mpa	Mpa	%	mm	mm	%
1 (Best from FEA)	27	190	9	10	0.127	13	162	166	2	0.37	0.3969	7
2 (Worst from FEA)	27	190	9	11	0	11	160	162	1.2	0.64	0.67	5
3 (Average FEA)	27	210	8	10	0.127	13	160	163	1.8	0.43	0.4471	4
4 (Optimized test)	27	190	8	10	0.127	11	165	168	1.7	0.26	0.2877	9.6

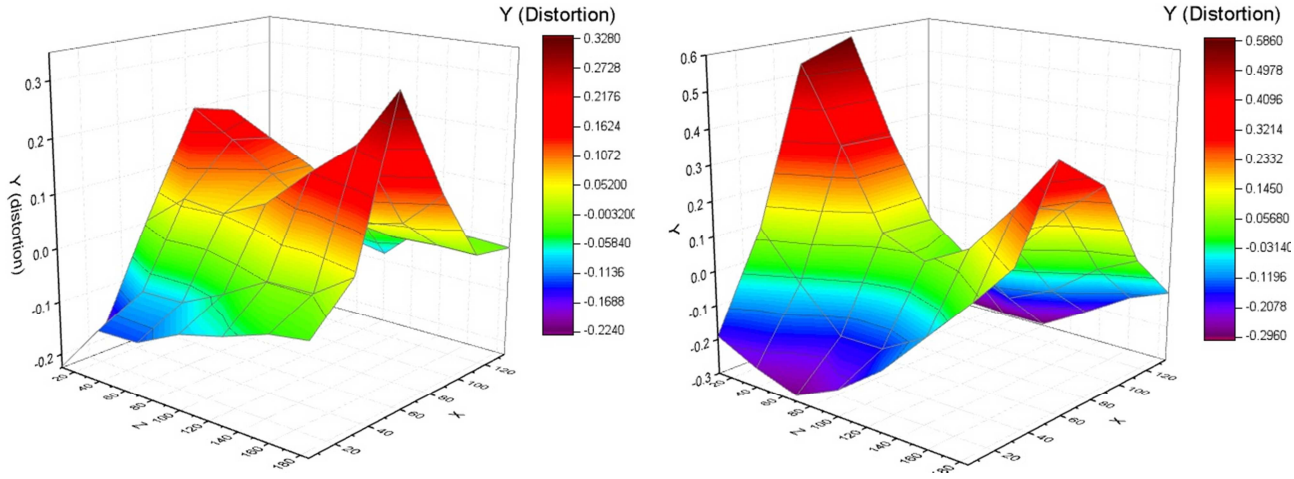

(a) (b)

Figure 11. *Deformation distribution on Y axes from experimental results measured by CMM machine (a) best sample number 1 (b) worst sample number.*

7. Discussion

Effect of Welding Parameters on Distortion:

Theoretically, when welding aluminum instead of carbon steel, some of the main things that cause distortion may have a bit more of an effect. As the results showed, the distortion of the weld is affected by more than just the weld parameters. It is also affected by the sample's schematic and joint preparation of the bevel angle. Based on the FEA results and the results of the experiments (Figure 12), test number 5 and 7 have less distortion than test number 6, even though test number 5 has more heat. The root gap is the difference between these two tests. A small root gap between two samples helps to reduce the distortion of the weld without having a big effect on penetration or UTS. The other important thing that effected distortion is distance between nozzle to weld. Based on the FEA, it can be seen that a 9.25-mm-thick sample can be welded with a 60-degree bevel angle, a 2.5-mm root face, and a butt-welded joint with only one pass, without any welding defects like the root and face not being welded properly. This is also shown by the experiment. With these results, industry could save a lot of time and money by making fewer passes with the same penetration (acceptance penetration according to all standards). Fewer passes, for sure, cause less distortion as well. The main goal of this search is to find the welding parameters that will allow full penetration with the fewest

number of passes. That goal has been met. The authors did a thorough review of the scientific literature and found that there is no sample that can be welded with 1.2 mm wire to a 9.25 mm sample in a single pass without any problems. So there is a direct relationship between the amount of heat change and the change in joint preparation when heated. When we arc-weld aluminum, we heat the material very quickly in a small area near the weld. Because of this, a small gap can help to reduce the distortion, as spread heat over the welds other than the new one. The correct sizing of the root face and bevel angle can help to reduce distortion. As a result of this search by using the American Welding Society and the Canadian Standard Association, a root face of 2.5 mm and a bevel of 60 degrees were chosen, and full penetration was achieved with this root penetration. The angle of the gun and the distance between the nozzle and the weld are two other important factors that affect distortion. As you can see, test number 3 has the least amount of heat. However, test number 8, which has almost the same parameters, has more heat than test number 3. The distance from the weld to the weld that is closer to the weld is the difference (11mm). Either test number 8 has more heat than test number 3, or test number 3 has less distortion. The reason is that when the nozzle is closer to the weld, most of the heat goes to the weld instead of the area around it.

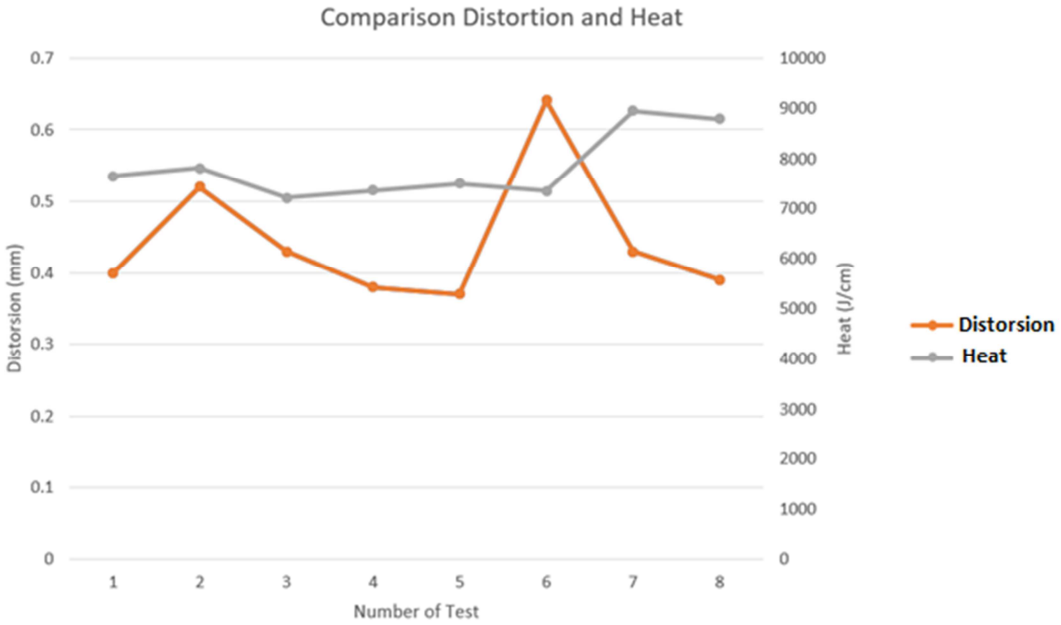

Figure 12. *Comparison between distortion and heat for all tests.*

8. Conclusions

This paper presents parameter optimization based on finite element analysis, ANN models, and experimental samples. Gas Metal Arc Welding is used in this study to weld two similar aluminum alloys, 6061 T6 with V groove weld, 60 degree bevel, and 2.5 mm root face. The results of this study can be summarized as follows:

1) Optimized parameters have been found for a 9.525 mm thick plate with a only one-pass weld that respects the minimum distortion and maximum UTS, as well as no surface defects
2) Experiments and FEA results have been compared and the error for distortion distribution is less than 10% and for temperature distribution is 5%, so there is a satisfactory agreement between the calculated weld simulation results and the experimental results.
3) Optimized parameter for voltage is 27v, Current 235, travel speed 8 mm/s, gun angle 10 degree, distance of the nozzle to weld 11 mm and root gap is 0.125 mm, in this situation the heat input is 7931.25 J/cm
4) FEA and experiment results have confirmed that in addition to voltage, travel speed, and wire feed speed, the distance of the nozzle to weld has a big effect on distortion and stress.

Funding

This research has been supported by funds of PI2 Team of laval university.

Conflicts of Interest

The authors declare no conflict of interest.

References

[1] R. O'brien, "Welding processes," in Welding Handbook, 1991, p. 91.

[2] M. Wahab, "Manual Metal Arc Welding and Gas Metal Arc Welding," Elsevier, 2014.

[3] A. Hernandez, G. Aguilera and M. Perez, "Welding sequence analysis in three dimensional weldments with experimental verification," Memorias del xxii congreso, pp. 367-387, 2016.

[4] F. Hosseinzadeh and P. Bouchard, "Mapping multiple components of the residual stress tensor in a large P91 steel pipe girth weld using a single contour cut," Experiment Mechanical Engineering, pp. 171-183, 2013.

[5] H. Huang, N. Ma and H. Murakawa, "Fast prediction of welding distortion using ism and i-ism with validation by experiment," in 4th International Ocean and Polar Engineering Conference, Korea, 2014.

[6] M. Chougule, M. Urhale, M. Walunj and A. Somase, "Study of thermally induced residual stresses for stainless steel grade using GMAW process," International Journal of Technology Enhancements and Emerging Engineering Research, vol. 2, pp. 17-21, 2014.

[7] D. Deng, "Influence of deposition sequence on welding residual stress and deformation in an austenitic stainless steel J-groove welded Joint," Material Design, vol. 49, pp. 1022-1033, 2013.

[8] D. Deng and S. Kiyoshima, "Influence of annealing temperature on calculation accuracy of welding residual stress in a SUS304 stainless steel joint," Acta Metallurgica Sinica, vol. 50, pp. 626-632, 2014.

[9] D. Deng, "Welding of dissimilar metals and post weld heat treatment," Encyclopedia of Thermal Stresses, 2014.

[10] Shen, W; Qiu, Y; Xu, L; Song, L, "Stress concentration effect of thin plate joints considering welding defects," Ocean Engineering, pp. 773-778, 2019.

[11] A. Nata and S. Babu, "Finite Element Simulation of Hybrid Welding Process for Welding 304 Austenitic Stainless Steel Plate," International Journal of Research in Engineering and Technology, vol. 1, pp. 101-120, 2012.

[12] M. Olson and M. Hill, "A new mechanical method for biaxial residual stress mapping," Experimental Mechanics, vol. 55, pp. 1139-1150, 2015.

[13] W. Perret, W. Schwent and M. Rethmeier, "Comparison of analytical and numerical welding temperature field calculation," Computational Materials Science, vol. 47, pp. 1005-1015, 2010.

[14] D. Qiao, W. Zhang, T. Pan and P. Crooker, "Evaluation of Residual Plastic Strain Distribution in Dissimilar Metal Weld by Hardness Mapping," Science and Technology of Welding and Joining, vol. 18, pp. 624-630, 2013.

[15] A. Yaghi, T. Hyde, A. Becker, W. Sun and J. Williams, "Residual stress simulation in thin and thick-walled stainless steel pipe welds including pipe diameter effects," International Journal of Pressure Vessels and Piping, vol. 83, pp. 864-874, 2011.

[16] S. Lewis, H. Alizadeh, H. Gill, C. Vega and H. Murakawa, "Modelling and measurement of residual stresses in autogenously welded stainless steel plates: Part 1—fabrication and modelling," International Journal of Pressure Vessels and Piping, vol. 12, no. 86, pp. 798-806, 2012.

[17] C. Xiz and B. Madigan, "Monte Carlo simulation and experimental measurements of grain growth in the heat affected zone of 304 stainless steel during multipass welding," The International Journal of Advanced Manufacturing, vol. 80, pp. 1197-1211, 2017.

[18] X. Shan, X. Davies, T. Wangsdan and N. O'Dowd, "Thermo-mechanical modelling of a single-bead-on-plate element method," International Journal of Pressure Vessels and Piping, vol. 86, pp. 110-121, 2009.

[19] M. Smith, J. Levesque, J. Bichler and L. Sediako,, "Residual stress analysis in linear friction welded in-service inconel 718 super alloy via neutron diffraction and contour method approaches," Material Science Engineering, pp. 168-179, 2017.

[20] S. Song and P. Dong, "Residual stresses at weld repairs and effects of repair geometry," Science and Technology of Welding and Joining, vol. 22, pp. 265-277, 2017.

[21] M. Kartal, Y. Kang and A. Korsunsky, "The influence of welding procedure and plate geometry on residual stresses in thick components," International Journal of Solids Structure, vol. 80, pp. 420-429, 2016.

[22] P. Kassab, "Experimental and finite element analysis of a T-joint welding," Journal of Mechanical Engineering and Automation, vol. 400, pp. 411-421, 2012.

[23] A. Yaghi, T. Hyde and A. Becke, "Finite Element Simulation of Residual Stresses Induced by the Dissimilar Welding of a P92 Steel Pipe with Weld Metal IN625," International Journal of Pressure Vessels and Piping, pp. 173-186, 2013.

[24] H. Yi, Y. Kim, J. Yoon and S. Kang, "Investigations on welding residual stress and distortion in a cylinder assembly by means of a 3d finite element method and experiments," Journal of Mechanical Science and Technology, vol. 25, pp. 3185-3193, 2011.

[25] A. Andrés, A. Alberto and J. Cardona, "Finite element modeling of welding processes," Applied Mathematical Modelling, vol. 707, no. 35, p. 688, 2011.

[26] "Simufact Software Manual," 2020.

[27] B. Yu and Y. Chen, "Driving rhythm method for driving comfort analysis on rural highways Promet Zagreb," TRID, vol. 4, no. 29, pp. 371-379, 2017.

[28] R. O'brien, Welding processes, Welding Handbook, vol. 2, American Welding Socity, 1991, p. 91.